Dynamics of the Cellular Metabolome during Human Cytomegalovirus Infection

Joshua Munger[1], Sunil U. Bajad[2], Hilary A. Coller[1], Thomas Shenk[1], Joshua D. Rabinowitz[2*]

1 Department of Molecular Biology, Princeton University, Princeton, New Jersey, United States of America, 2 Department of Chemistry and Lewis-Sigler Institute for Integrative Genomics, Princeton University, Princeton, New Jersey, United States of America

Viral replication requires energy and macromolecular precursors derived from the metabolic network of the host cell. Despite this reliance, the effect of viral infection on host cell metabolic composition remains poorly understood. Here we applied liquid chromatography-tandem mass spectrometry to measure the levels of 63 different intracellular metabolites at multiple times after human cytomegalovirus (HCMV) infection of human fibroblasts. Parallel microarray analysis provided complementary data on transcriptional regulation of metabolic pathways. As the infection progressed, the levels of metabolites involved in glycolysis, the citric acid cycle, and pyrimidine nucleotide biosynthesis markedly increased. HCMV-induced transcriptional upregulation of specific glycolytic and citric acid cycle enzymes mirrored the increases in metabolite levels. The peak levels of numerous metabolites during infection far exceeded those observed during normal fibroblast growth or quiescence, demonstrating that HCMV markedly disrupts cellular metabolic homeostasis and institutes its own specific metabolic program.

Citation: Munger J, Bajad SU, Coller HA, Shenk T, Rabinowitz JD (2006) Dynamics of the cellular metabolome during human cytomegalovirus infection. PLoS Pathog 2(12): e132. doi:10.1371/journal.ppat.0020132

Introduction

Host cells provide viruses with the metabolic resources necessary for their replication. Viral replication requires bulk macromolecule synthesis, which depends on a substantial supply of biopolymer subunits and energy for their assembly. Anti-viral compounds that target viral utilization of macromolecular precursors, such as nucleotide analogs, have proven to be successful clinical treatments. Notwithstanding these therapeutic successes, the mechanisms through which viruses engage and manipulate the small molecule metabolic network of host cells remain largely a mystery.

Human cytomegalovirus (HCMV) is a prototypical β-herpes virus family member. Epidemiological studies have demonstrated that the virus is widespread, infecting more than half of the earth's population [1]. Most healthy adults undergo an asymptomatic infection, during which the virus enters a latent state for the life of its host. However, primary infection or reactivation of latent HCMV causes life-threatening disease in immunologically immature or compromised individuals. In addition, HCMV is the leading known infectious cause of birth defects; congenital infection can result in multiple organ system abnormalities with damage to the auditory system occurring in the majority of symptomatic newborns [1].

Like all herpesviruses, the HCMV particle is enveloped and contains a large double-stranded DNA genome packaged inside a protein capsid. The capsid in turn is surrounded by a protein tegument layer residing between the capsid and the envelope.

HCMV infection induces total RNA and protein synthesis in infected cells [2,3]. However, it remains unclear to what extent HCMV infection perturbs small molecule metabolism to accomplish the macromolecular synthesis needed for viral replication. Here we used liquid chromatography-tandem mass spectrometry (LC-MS/MS) to measure the levels of 63 different intracellular metabolites during HCMV infection of cultured fibroblasts. Additionally, to provide insight into potential transcriptional activation of metabolic pathways, we conducted mRNA expression profiling in parallel.

We find that as infection progresses, the levels of numerous metabolic components in pathways such as glycolysis, the tricarboxylic acid (TCA) cycle, and pyrimidine biosynthesis markedly increase. Mirroring our metabolomics data, HCMV transcriptionally activates genes encoding components of the TCA cycle, glycolytic pathway, and certain aspects of the pyrimidine biosynthetic pathway. The peak levels of various metabolites during infection far exceed those observed during normal fibroblast growth or quiescence, indicating that HCMV markedly disrupts metabolic homeostasis.

Results/Discussion

Cell Handling and Metabolite Extraction

LC-MS/MS data on 167 different metabolites were collected at various times following infection with HCMV or a mock negative control innoculum. Fibroblasts were grown to confluence and then maintained in serum-free medium for 24 h prior to infection. This treatment served to synchronize

Editor: Beth Levine, University of Texas Southwestern Medical Center, United States of America

Received June 29, 2006; **Accepted** November 2, 2006; **Published** December 15, 2006

Abbreviations: CAD, carbamoyl phosphate synthetase-aspartate transcarbamoylase-dihydroorotase; DHAP, dihydroxyacetone phosphate; FBP, fructose bisphosphate; HCMV, human cytomegalovirus; hpi, hours post infection; LC-MS/MS, liquid chromatography-tandem mass spectrometry; PEP, phosphoenolpyruvate; qPCR, quantitative PCR; SRM, selected reaction monitoring scan event; TCA, tricarboxylic acid

* To whom correspondence should be addressed. E-mail: joshr@genomics.princeton.edu

Synopsis

Viruses are parasites. They depend on the biochemical infrastructure of host cells to grow. A key element of the infrastructure provided by the host cell is its metabolic machinery, which viruses rely upon to provide the energy and building blocks necessary for their replication. The way in which viruses interact with host cell metabolism remains, however, poorly understood. The authors have used an advanced measurement technique, liquid chromatography-mass spectrometry, to quantitate directly the levels of a large number of metabolic compounds (energy molecules and biochemical building blocks) during cytomegalovirus infection of cultured human cells. They find that viral infection leads to dramatic increases in the levels of many metabolites and that these increases substantially exceed those associated with normal transitions of cells between resting and growing states. In several cases, enhanced metabolite levels induced by the virus coincide with an apparent increase in host cell production of the machinery (enzymes) involved in making those metabolites. This work represents the first comprehensive characterization of the metabolic environment of virally infected cells and identifies a number of profound metabolic effects of the virus, some of which may eventually prove fruitful targets for antiviral therapy.

the cells in G0 (Figure S1), which reduces cell-to-cell variation in response to infection [4]. Additionally, the use of serum-free medium removes a complex source of extraneous metabolites from the analysis. Cells were assayed at 4, 24, 48, 72, and 96 h post infection (hpi) to provide coverage during the extended replication cycle of HCMV. In cultured fibroblasts, viral gene expression is first detected at about 2 hpi, viral DNA replication begins between 24–30 hpi, and peak virus yields are achieved between 72–96 hpi, after which the cells die.

At the appropriate time post infection, medium was aspirated from the cells (a thin film of medium remains covering the cells due to surface tension effects, avoiding alteration of the immediate cellular environment) and −75 °C methanol was immediately added to quench metabolic activity and extract metabolites. Given the speed of metabolic reactions, quickly removing medium and immediately quenching metabolism is essential for obtaining reliable results; we have found that even a single wash step leads to substantial changes in metabolome composition. The selection of cold methanol as an extraction solvent was based on systematic studies in bacteria and yeast, which point to its providing relatively good extraction of a broad spectrum of metabolites [5–7], while avoiding marked metabolite decomposition and associated formation of decomposition products, which can themselves mimic metabolites [8]. A contributor to the efficacy of −75 °C methanol as an extraction solvent is likely its disrupting membranes by inducing formation of microscopic ice crystals.

Metabolite Quantitation

Extracted metabolites were measured via LC-MS/MS, with the LC separation involving hydrophilic interaction chromatography on an aminopropyl resin at basic pH, an approach tailored to quantitation of water-soluble cellular metabolites [9]. Each metabolite measurement was in the form of a selected reaction monitoring scan event (SRM); formation within the mass spectrometer collision cell of a particular molecular weight product ion from a specific molecule weight parent ion by gas phase collision of the parent ion with argon occurring at a specific chromatographic retention time. These SRMs were designed based on prior knowledge of the retention time and mass spectrometry fragmentation pattern of a purified standard of the metabolite of interest [6], with a one-to-one correspondence between metabolites and SRMs. An exception to the one-to-one relationship between metabolites and SRMs was the co-elution of certain metabolite isomers yielding identical fragmentation patterns (e.g., different isomers of glucose-6-phosphate, which we refer to collectively as hexose-phosphate).

In many cases, no useful quantitative data were obtained, due to the metabolite never being present in detectable amounts or being present in the medium at such high levels as to interfere with analysis. For 63 metabolites, however, reliable quantitative data were obtained in the form of ion counts from compound-specific SRM chromatograms (for details on the requirements for metabolite inclusion see Materials and Methods). These 63 metabolites included a variety of key components of central carbon metabolism and nucleotide metabolism, including multiple phosphorylated compounds such as ATP and fructose bisphosphate (FBP).

Internal Standards

To ensure that experimental artifacts such as ion suppression did not lead to misinterpretation of metabolite levels, isotope-labeled internal standards were added to every sample. As is typical for electrospray ionization-mass spectrometry data, there are occasional fluctuations in the internal standard signals, generally in the range of ~20% (Figure S2), which is much smaller than the effects due to viral infection described below. As the fluctuations generally occurred in parallel for the mock versus viral samples and did not follow any systematic pattern with respect to viral versus mock treatment (Figure S2), there is no evidence of systematic error between mock and viral samples due to ion suppression or other electrospray ionization-mass spectrometry artifacts. Accordingly, experimental error in the LC-MS/MS measurement is very unlikely to have influenced the biological conclusions of the present work.

Data Normalization and Presentation

To enable cross-sample comparison of metabolite (ion count) signals, the observed signal was normalized with respect to the total protein content of the cells used to generate the sample. Protein content, rather than cell number, was used for normalization because HCMV-infected cells increase approximately 2-fold in volume as compared to mock-infected cells. Normalization with respect to protein content should yield signals in units approximating ion counts/cell volume, which for any given metabolite is linearly proportional to its intracellular concentration [9]. Comparison of ion counts across compounds is complicated by compound-specific ionization efficiencies. Accordingly, signals were further normalized to the initial (t = 4 h) signal in the mock-infected condition.

Time course data for compounds or pathways of particular interest are shown in Figures 1–6, and complete data (including absolute ion counts) on the 63 quantifiable metabolites are provided in Table S1. RNA expression data were collected by microarray analysis, and data for key

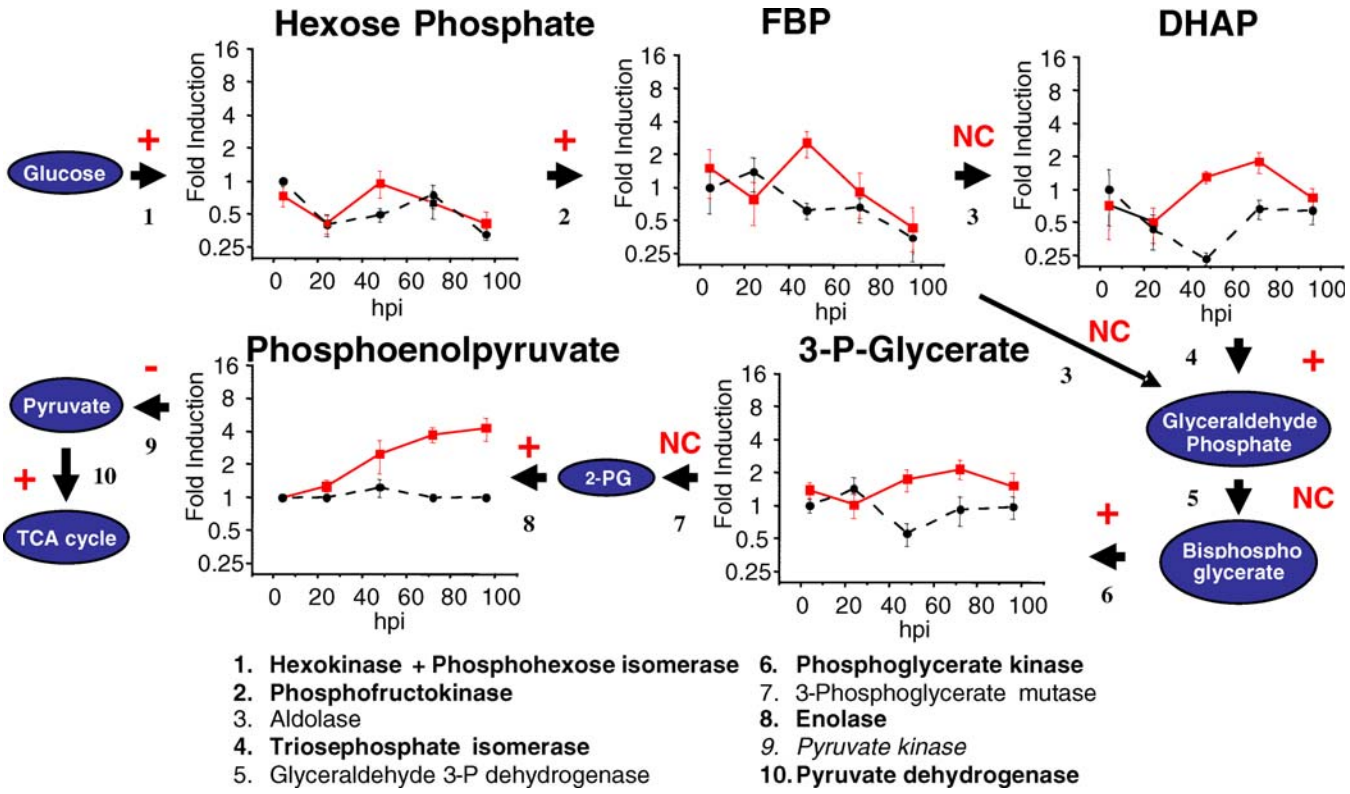

Figure 1. HCMV-Induced Changes in Glycolytic Metabolites

Replicate cultures of confluent fibroblasts were serum-starved for 24 h and subsequently mock- infected (dotted line) or virally infected at a multiplicity of 3.0 pfu/cell with HCMV (red line). Cells were harvested at 4, 24, 48, 72, and 96 hpi and processed for LC-MS/MS. SRM peak heights from two independent experiments performed in duplicate ($n = 4$) were normalized to protein levels. Average fold change in the metabolite level (relative to the mock 4-h sample) is plotted on a $\log_2$ axis. Error bars show $\pm$ 1 SE of the mean. Transcriptional data are depicted graphically at the relevant enzymatic step by the following symbols (shown in red): +, increased and –, decreased $\geq$1.5-fold in HCMV infection versus mock infection and $p < 0.05$ based on ANOVA analysis; NC, no change, either not significant by ANOVA or effect of HCMV < 1.5-fold. Enzyme names are also provided, with those increased transcriptionally listed in bold and those decreased in italics. Transcriptional data represent an average across 24, 48, and 72 h and specific enzyme isoforms/subunits.

doi:10.1371/journal.ppat.0020132.g001

metabolic enzymes that changed significantly upon infection are shown in Figure 7. The primary expression data are provided in full via the Princeton University MicroArray database (http://puma.princeton.edu/index.shtml). In certain specific cases, we validated our microarray data using quantitative PCR (qPCR) (Figure 2A).

General Strategies for Data Interpretation

Before addressing particular experimental observations, it is useful to consider the different potential causes of particular metabolite level changes. Consider the following metabolic pathway:

$$A \rightarrow B \rightarrow C$$

Increased intracellular levels of a given metabolite B can arise from either increased flux from A → B, or decreased flux from B → C. These alternatives can likely best be distinguished using isotope tracers; however, in the absence of such tracer data (which will not be presented here), good estimates of the true cause of a change in the level of metabolite B can often be made based on knowledge of key regulated steps in metabolic pathways. That is, if the reaction A → B but not B → C is known to be a key regulated step, then change in flux through A → B likely accounts for the change in the level of B. For example, in Figure 1 we report an increase in FBP at 48 hpi. As production of FBP via phosphofructose kinase-1(PFK-1) is tightly regulated [10–12], whereas consumption of FBP by aldolase is not, the most likely cause of the increase in FBP is increased PFK-1 flux. This conclusion is reinforced by the observation that levels of the aldolase product, dihydroxyacetone phosphate (DHAP), increase roughly in parallel with those of FBP (if the increase in FBP were due to blockade of aldolase, DHAP levels should drop, not increase). It is confirmed by direct measurement of PFK activity from cell lysates, as described further below (Figure 2B).

The above analysis considers only the two most basic causes of changes in the level of metabolite B: altered consumption or production via a linear pathway. It is worth noting that especially in a highly compartmentalized eukaryotic cell, other situations can arise. For example, imagine that the reactions A → B → C normally occur in a subcellular compartment that upon viral infection begins to leak B into the cytosol, which contains no enzyme that consumes B. In this case, increased levels of B may occur independently of flux increases or decreases via the standard A→ B → C reaction pathway, depending instead on the extent of B leakage. Such a case may describe the pyrimidine pathway intermediate carbamoyl-aspartate, as will be discussed later.

We wish to emphasize that while transport of metabolites between subcellular compartments may play a key role in

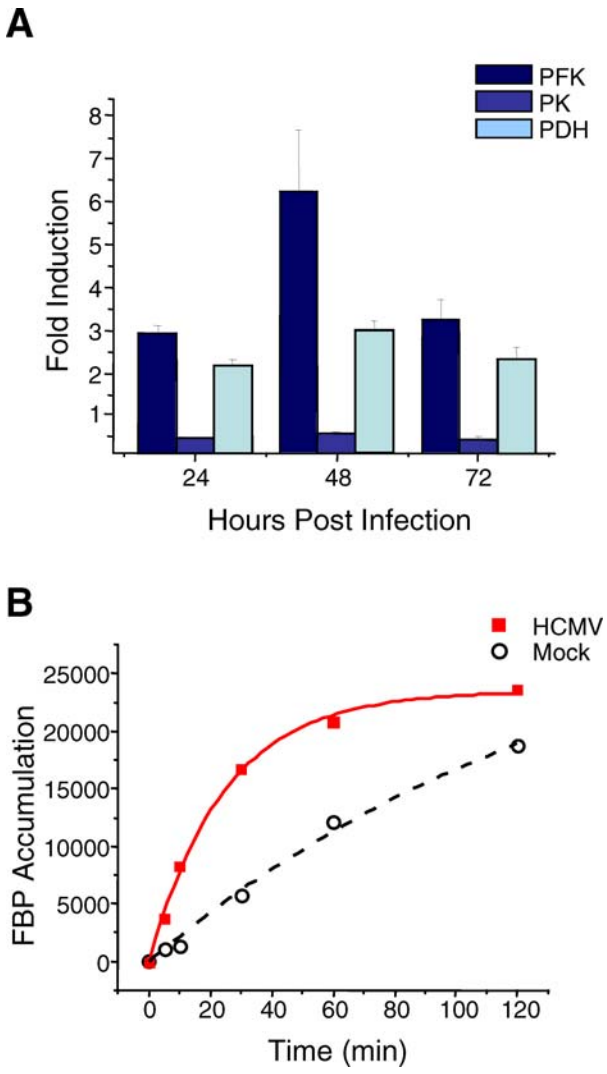

Figure 2. HCMV-Induced Changes in Metabolic Enzyme Activity and Transcript Levels

(A) Levels of metabolic mRNA transcripts during HCMV infection. Transcript levels for phosphofructokinase-1(PFK), pyruvate kinase (PK), and pyruvate dehydrogenase (PDH) were assayed at 24, 48, and 72 h post-mock or post-HCMV infection by qPCR. Bars represent the mean levels ($n = 2$) in the HCMV-infected cells divided by those in the mock-infected cells at the indicated time point, with the error bars showing +1 SD of the mean.

(B) HCMV induction of phosphofructokinase activity. FBP accumulation was measured in mock-infected (dotted line) and HCMV-infected (red line) cellular lysates collected at 48 hpi. Similar results were found in three independent experiments.

doi:10.1371/journal.ppat.0020132.g002

regulation of mammalian metabolism, our current analytical approach provides only average metabolite levels throughout the full cellular volume. Accordingly, the pathway diagrams in the figures include only covalent, not transport, reactions.

Effect of HCMV Infection on Upper Glycolysis

Glycolysis and the TCA cycle oxidize hexose sugars to form ATP and NADH, the major energy currencies of the cell. While HCMV infection has been previously shown to stimulate glucose uptake in fibroblasts [13], its detailed effect on intracellular carbon metabolism has not been previously investigated.

We found that early during infection (i.e., 4–24 hpi), there was little difference in measurable glycolytic pathway metabolites between mock- and HCMV-infected fibroblasts (Figure 1). Beginning at 48 hpi, however, differences emerged: FBP, DHAP, 3-phosphoglycerate, and phosphoenolpyruvate (PEP) increased relative to mock infection (Figure 1).

The increased levels of glycolytic intermediates during HCMV infection correlated with an increase in the transcript levels of several glycolytic enzymes (Figures 1 and 7). One such enzyme, PFK-1, is the key upstream regulator of glycolytic flow [14–16]. To verify our microarray results regarding this important regulatory enzyme, we analyzed its transcript levels over the course of infection by qPCR. Transcript levels were found to be increased at every time point assayed with a peak 6-fold increase at 48 hpi (Figure 2A). The levels of PFK-1′s product, FBP, also peaked at this time, suggesting increased PFK-1 activity in HCMV-infected cells at 48 hpi. To directly test for such activity, we performed biochemical assays on cell lysates. Addition of fructose-6-phosphate and ATP to lysates of HCMV-infected or mock-infected cells resulted in accumulation of FBP, with the initial rate of accumulation ~4-fold greater for HCMV than mock infection. Since PFK-1 regulates glycolytic flow, the increased levels of downstream glycolytic intermediates during HCMV infection likely reflect, at least in part, this increase in PFK-1 activity.

Glycolytic Efflux during HCMV Infection

Most of the measured glycolytic intermediates increased at 48 hpi relative to their status in mock-infected cells. However, the increase in FBP was transient, presumably due to its rapid conversion to downstream glycolytic intermediates. The terminal glycolytic metabolite, PEP, increased from 48 hpi onward (Figure 1). This suggested the presence of a bottleneck to glycolytic efflux at the level of pyruvate kinase late in infection. Such a bottleneck could arise from decreased maximum velocity for the pyruvate kinase reaction (e.g., due to decreased pyruvate kinase levels), increased K_m of the enzyme for PEP (e.g., due to allosteric regulation or shift to a higher K_m isozyme), or failure of pyruvate kinase activity to keep pace with increased flux through upper glycolysis. Our microarray data revealed increased expression of enzymes linking FBP to PEP (triose phosphate isomerase, phosphoglycerate kinase, and enolase) but decreased expression of pyruvate kinase (Figures 1, 2A, and 7). This decrease in pyruvate kinase transcript is consistent with (and may potentially cause) the observed accumulation of PEP. Note that the reactions linking DHAP to PEP are associated with net $\Delta G^{0\prime}$ ~zero [17]. Thus, irrespective of the activities of the intervening enzymes, DHAP and its products must accumulate in parallel with PEP for glycolysis to continue to run in the net forward direction.

The principal carbohydrate product of glycolysis is pyruvate, which was not measured here due to its poor fragmentation in MS/MS. A key metabolite of pyruvate is alanine, which is produced via pyruvate transamination. Levels of alanine increase markedly starting at 48 hpi (Figure 3), in concert with the increase in FBP and other glycolytic intermediates (Figure 1). Much like PEP, alanine levels grow steadily from 48 hpi onward. This suggests that overall glycolytic flux (as reflected in part by alanine production) is increased from 48 hpi onward, with shifting enzymatic

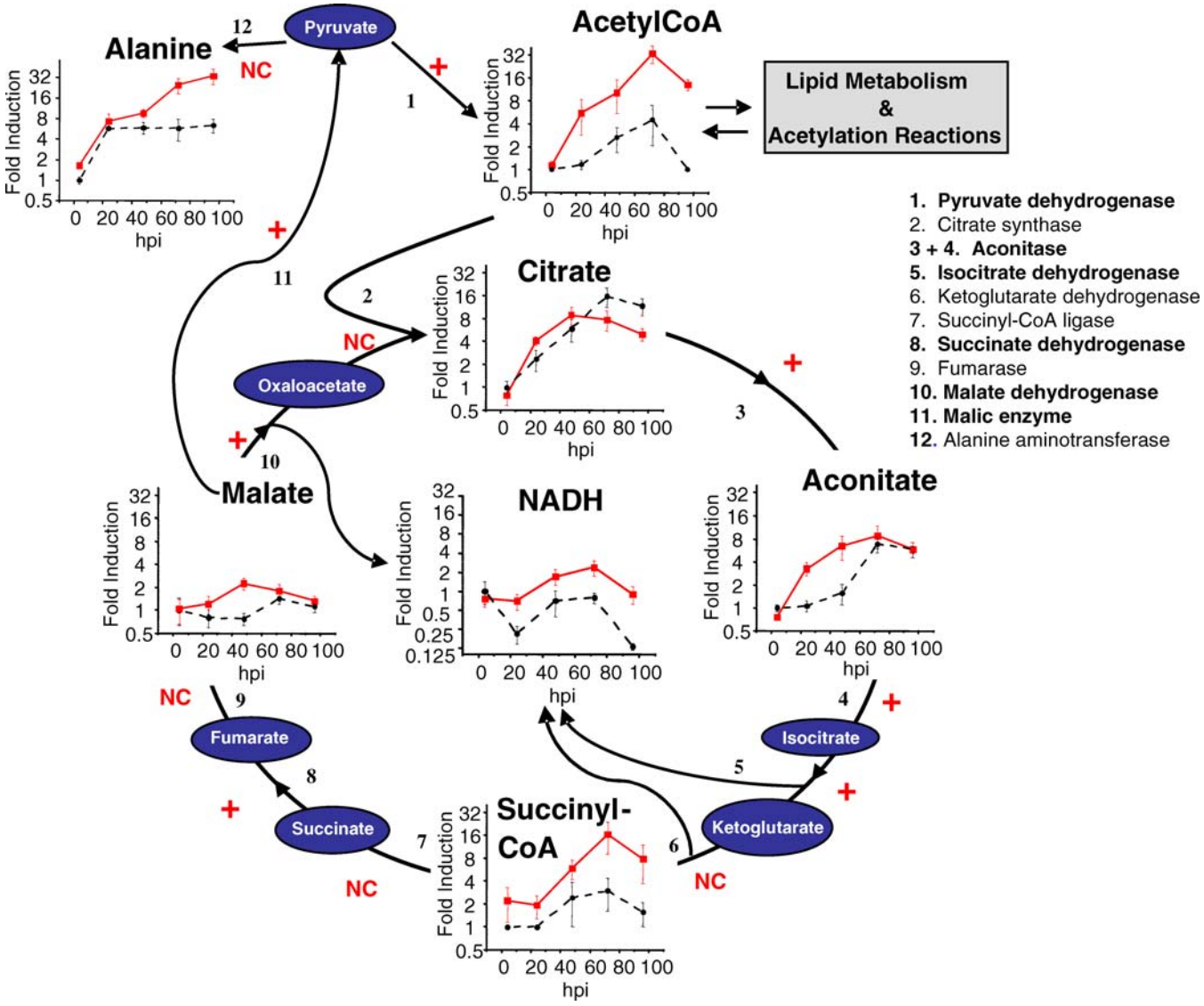

Figure 3. HCMV-Induced Changes in the TCA Cycle

Metabolite data from mock-infected (dotted line) or virally infected (red line) fibroblasts are plotted, with the symbols + and NC (shown in red) over the arrows indicating changing levels of enzyme transcripts as described in the Figure 1 legend.

doi:10.1371/journal.ppat.0020132.g003

activity in lower glycolysis altering the balance of FBP versus PEP during this period.

Intriguingly, two common features of human cancers are the activation of phosphofructokinase activity mediated by increased F2,6P accumulation and the expression of a particularly low-activity isozyme of pyruvate kinase [11,18,19]. Thus, increased phosphofructokinase activity and decreased pyruvate kinase activity, which together may favor use of glycolytic intermediates for production of biosynthetic building blocks, appear to be shared between cancer and HCMV infection.

Increased Acetyl-CoA during HCMV Infection

Acetyl-CoA occupies a central position in metabolism. It is the link between glycolysis and the TCA cycle, as well as a hub for fatty acid and amino acid oxidation and de novo lipid biosynthesis. Like alanine, acetyl-CoA can be formed from pyruvate, and like alanine, acetyl-CoA increased dramatically throughout HCMV infection; however, acetyl-CoA is unique in rising even before glycolytic intermediates and ultimately increasing by ~8-fold in infected as compared to uninfected cells (Figure 3). The strength of the acetyl-CoA response, as well as its initiation prior to evidence of increased glycolytic intermediates, suggests the possibility of increased activity of the key acetyl-CoA producing enzyme complex, pyruvate dehydrogenase. Consistent with this notion, pyruvate dehydrogenase transcript levels were upregulated 2- to 3-fold by the virus both by microarray (Figure 7) and by qPCR (Figure 2).

TCA Intermediates during HCMV Infection

When acetyl-CoA enters the TCA cycle, it is converted, with the addition of oxaloacetate, into citrate. Throughout infection, the levels of many TCA cycle constituents were increased with respect to mock infection; however, citrate levels were not, although citrate levels did increase in parallel in both mock- and virus-infected samples (Figure 3). Citrate

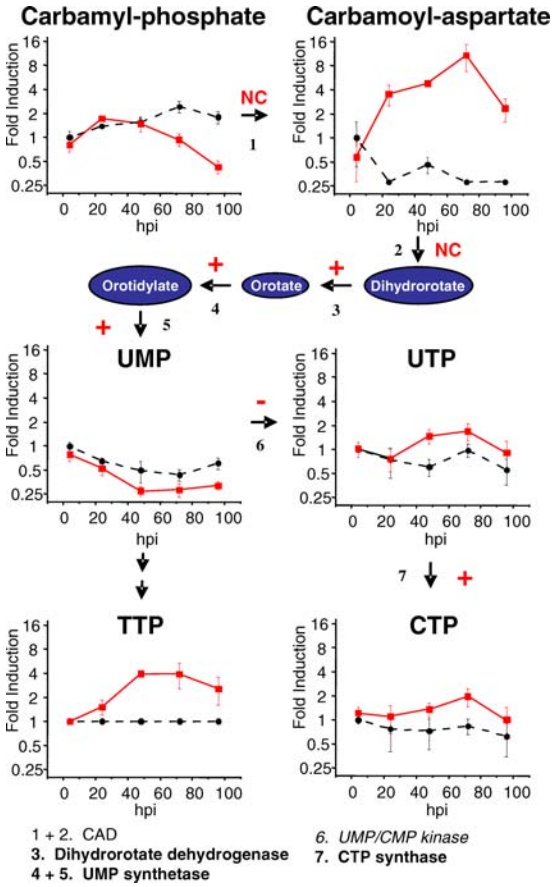

Figure 4. HCMV-Induced Changes in Pyrimidine Biosynthesis

Metabolite data from mock-infected (dotted line) or virally infected (red line) fibroblasts are plotted, with the symbols +, −, and NC (shown in red) over the arrows indicating changing levels of enzyme transcripts as described in the Figure 1 legend.

doi:10.1371/journal.ppat.0020132.g004

synthase activity is inhibited by increased levels of NADH and succinyl-CoA [20], the levels of which are elevated during HCMV infection (Figure 3), potentially preventing accumulation of citrate (Figure 3). Alternatively, oxaloacetate may be diverted via aspartate into de novo pyrimidine synthesis, which is activated during HCMV infection (Figure 4), thus limiting its availability for citrate synthesis; direct oxaloacetate measurement here was precluded by oxaloacetate instability [9]. More likely, however, citrate synthase flux was increased as a consequence of increased acetyl-CoA levels, but citrate levels were kept steady by increased activity of the citrate-consuming enzyme, aconitase, whose mRNA level increased during HCMV infection (Figure 7). Consistent with increased aconitase expression, aconitate (4-fold increased at 24 and 48 hpi) and its downstream TCA cycle products, including succinyl-CoA and malate, increased during infection (Figure 3). Because succinyl-CoA is the entry point for odd-numbered fatty acid chains into central carbon metabolism, its particular strong induction hints at the possibility of increased fatty acid catabolism induced by the virus. Transcriptionally, the expression levels of malic enzyme and malate dehydrogenase both increased (Figure 7). Malic enzyme converts malate to pyruvate, potentially contributing to increased alanine and acetyl-CoA levels and limiting citrate levels, whereas malate dehydrogenase produces oxaloacetate from malate, thus completing the TCA cycle by providing citrate synthase with oxaloacetate.

The primary recipient of the energy released from citric acid cycle oxidations is the reduced electron carrier NADH. Consistent with elevated glycolysis and citric acid cycle activity, NADH levels increased approximately 2- to 4-fold relative to mock infection at every time assayed after 4 h (Figure 3). This increase in NADH was unlikely to be due to reduced NADH consumption, as enzymes of the electron transport chain and the ATP-synthesizing proton pump were markedly transcriptionally upregulated (Table S2). Taken together, these results are most consistent with the hypothesis that HCMV infection stimulates both glycolytic and pyruvate dehydrogenase flux. This could generate the observed high level of acetyl-CoA, which was then used to drive the TCA cycle to produce NADH and eventually ATP, as well as potentially also donating carbon units to lipid biosynthesis, which was not explored here.

Dynamics of Central Carbon Metabolites in the Absence of HCMV

The levels of certain compounds, e.g., citrate, aconitate, and alanine, increased during mock infection (Figure 3). The levels of other compounds, e.g., FBP and NADH, decreased (Figures 1 and 3). As the cellular medium was not changed during the course of infection, these changes may reflect alteration of the cellular nutrient environment over time, perhaps due to glucose becoming less abundant and glycolytic waste products accumulating. Alternatively, the changes in metabolite levels may reflect long-term adaptations of fibroblasts to tissue culture. One effect of HCMV infection may be to accelerate some of these processes that occur even in its absence; however, acceleration of normal physiological processes is inadequate to account fully for the profound and persistent changes seen in many compounds such as acetyl-CoA and NADH.

HCMV Manipulation of Pyrimidine Biosynthesis

HCMV infection stimulates total RNA and DNA synthesis and increases the total number of cellular ribosomes without degrading host cell chromosomal DNA [2]. Consequently, the virus must induce substantial de novo nucleotide biosynthesis. The first three steps of pyrimidine biosynthesis are catalyzed in eukaryotes by a homo-trimer of the 230-kDa protein termed carbamoyl phosphate synthetase-aspartate transcarbamoylase-dihydroorotase (CAD), which catalyzes the synthesis of carbamoyl-phosphate, carbamoyl-aspartate, and dihydroorotate [21–23]. Carbamoyl-phosphate levels remained relatively similar in mock-infected cells versus HCMV-infected cells until 72 h when they started to fall in infected fibroblasts (Figure 4). Levels of carbamoyl-aspartate, in contrast, increased dramatically during viral infection starting at 24 hpi (Figure 4). While levels of carbamoyl-aspartate increased substantially, levels of the CAD transcript remain unchanged during the course of infection (Figure 4), suggesting that transcriptional activation of the CAD gene is not responsible for the accumulation of carbamoyl-aspartate. The increased carbamoyl-aspartate levels did not appear to arise from blockade in its utilization, as levels of pyrimidine biosynthetic end products such as the ribonucleotides UTP and CTP and the deoxyribonucleotide TTP were generally

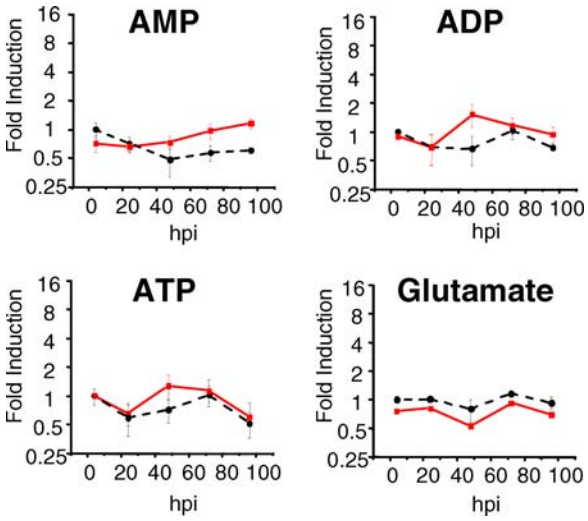

Figure 5. Homeostasis of Purine Nucleotides and Amino Acids during HCMV Infection

Metabolite data from mock-infected (dotted line) or virally infected (red line) fibroblasts are plotted as described in the Figure 1 legend.
doi:10.1371/journal.ppat.0020132.g005

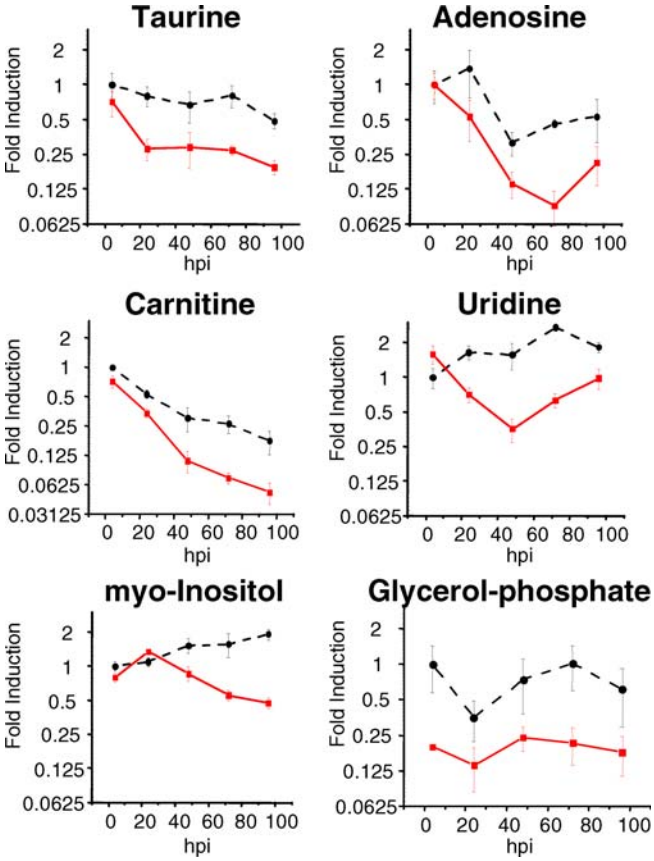

Figure 6. HCMV-Induced Decreases in Selected Metabolite Pools

Metabolite data from mock-infected (dotted line) or virally infected (red line) fibroblasts are plotted as described in the Figure 1 legend.
doi:10.1371/journal.ppat.0020132.g006

increased compared to mock infection (Figure 4), although levels of UMP, which sits in the middle of pyrimidine biosynthesis, were actually slightly decreased.

Interestingly, UTP reportedly serves as a feedback inhibitor of CAD activity [24,25] and one would expect that the increased levels of UTP that occur during HCMV infection might inhibit CAD activity, thereby blocking carbamoyl-aspartate accumulation. One possible explanation for the continued high levels of carbamoyl-aspartate in the face of high UTP is that infection might spatially segregate UTP and CAD into different compartments. This might involve interplay between the virus and mitogen-activated protein kinase, which has recently been shown to regulate CAD activity/localization [26].

Another challenge in interpreting the carbamoyl-aspartate accumulation is that the three active sites of CAD are linked by a 96-Å long channel which supposedly localizes carbamoyl-phosphate and carbamoyl-aspartate to the interior of the enzyme [27–29]. Thus, the presence of free carbamoyl-aspartate may indicate profound perturbation of CAD in infected cells, perhaps as the consequence of an interacting virus-coded protein that results in leakage of carbamoyl-aspartate from the enzyme interior.

Purine Homeostasis during HCMV Infection

In contrast to the aforementioned alterations of the pyrimidine biosynthetic pathway, HCMV infection did not dramatically affect purine metabolite pool levels. AMP, ADP, and ATP metabolite levels did not change significantly with respect to mock infection, with the exception of a slight increase in ADP and ATP at 48 h and a small accumulation of AMP after 48 h in HCMV-infected versus mock-infected fibroblasts (Figure 5). The present study does not provide substantial insight into de novo purine biosynthesis however, because the only purine intermediate for which an SRM was included, IMP, could not be measured due to interference from naturally occurring heavy isotopes of AMP (see Materials and Methods). While the levels of purines do not change dramatically, it is likely that increased turnover of the high-energy phosphate bond of ATP occurs, as the RNAs encoding mitochondrial ATP synthases were significantly upregulated (Table S2).

The dramatic increase in pyrimidine versus purine levels may reflect different biological roles of the two families of metabolites. Dramatic concentration changes in ATP and GTP could alter the balance of a multitude of enzymatic reactions and interactions based on their widespread utilization as signaling constituents and energy currency. As such, a pathogen may be forced to maintain purine levels close to normal physiological levels. Pyrimidines, in contrast, do not have equally wide-ranging functions and thus HCMV may have license to more dramatically influence pyrimidine levels.

HCMV Infection and Amino Acids

With the exception of alanine, HCMV infection did not induce increased levels of other measured amino acids. While the presence of exogenous amino acids in the medium precluded quantification of a number of amino acids, the levels of glutamate were not affected by viral infection (Figure 5), nor were the levels of asparagine, aspartate, histidine, or proline (Table S1). Taken together, these data suggest that while HCMV infection strongly impacts the metabolite levels of certain metabolites, it has little effect on many amino acid levels.

Pathway	Probe[a]	Common Name	24–72 h Average[b]	Isozyme Average[c]
Glycolysis	A_24_P108451	Glucose phosphate isomerase	2.0	
	A_23_P29081	Phosphofructokinase, liver	0.8	1.5
	A_23_P46928	Phosphofructokinase, platelet	2.1	
	A_32_P95739	Triosephosphate isomerase 1	2.1	1.9
	A_23_P53546	Triosephosphate isomerase 1	1.7	
	A_24_P604649	Phosphoglycerate kinase 1	1.9	2.0
	A_23_P125829	Phosphoglycerate kinase 1	2.0	
	A_23_P137391	Enolase 1 alpha	1.6	3.2
	A_24_P105501	Enolase 1 alpha	1.6	
	A_24_P236091	Enolase 2 gamma, neuronal	6.4	
	A_23_P399501	Pyruvate kinase, muscle	0.7	0.6
	A_32_P147241	Pyruvate kinase, muscle	0.6	
	A_23_P251095	Pyruvate dehydrogenase alpha 1	2.2	
TCA	A_23_P305481	Aconitase 2, mitochondrial	2.9	2.8
	A_23_P103149	Aconitase 2, mitochondrial	2.8	
	A_23_P140668	Isocitrate dehydrogenase 3 alpha	1.8	1.8
	A_24_P167806	Isocitrate dehydrogenase 3 alpha	2.0	
	A_23_P502196	Isocitrate dehydrogenase 3 beta	1.7	
	A_23_P166068	Isocitrate dehydrogenase 3 beta	1.6	
	A_23_P79545	Succinate-CoA ligase, alpha subunit	1.8	1.2
	A_23_P99249	Succinate-CoA ligase, beta subunit	0.6	
	A_32_P67259	Succinate dehydrogenase, subunit A	1.7	2.3
	A_23_P149649	Succinate dehydrogenase, subunit B	2.9	
	A_23_P31372	Malate dehydrogenase 2, NAD mitochondrial	2.4	
	A_23_P422026	Malic enzyme 1, NADP(+)-dependent, cytosolic	1.6	
Pyrimidine	A_23_P21706	CTP synthase	1.8	
	A_23_P15202	Dihydroorotate dehydrogenase	1.6	
	A_23_P115366	UMP-CMP kinase	0.6	
	A_23_P6624	UMP synthetase	2.5	

Figure 7. Effect of HCMV on RNA Levels of Glycolytic, TCA Cycle, and Pyrimidine Biosynthetic Enzymes

Transcriptional data that passed variance analysis (ANOVA, $p < 0.05$).

[a]More information on specific genes can be accessed using probe designations at http://www.reactome.org.

[b]Average fold induction over mock infection (averaged over 24, 48, and 72 hpi).

[c]Represents averaged isozyme/subunit induction over mock in cases where data for multiple isozymes/subunits exist.

doi:10.1371/journal.ppat.0020132.g007

HCMV Infection Depletes Cells of a Subset of Metabolites

A number of metabolites were found to decrease rapidly during HCMV infection compared to mock infection of fibroblasts (Figure 6). These metabolites could be grouped generically into those, such as adenosine and carnitine, for which HCMV infection seemed to accelerate decreases that also occurred during mock infection, and others, like myo-inositol and glycerol phosphate, which decreased only in the HCMV infection condition. Several of the metabolites decreasing during HCMV infection were nucleosides (adenosine and uridine), consistent with use of these metabolites for nucleotide and eventually RNA or DNA biosynthesis. Others were related to lipid metabolism: carnitine, which plays a key role in β-oxidation of long-chain fatty acids [30,31]; glycerol-phosphate, a precursor to the glycerol portion of phospholipids, diacylglycerols, and triglycerides; and myo-inositol, a precursor to inositol-containing lipids such as phosphatidyl-inositol. The results for glycerol-phosphate, while unusually noisy, were striking in that decreases were evident already at 4 hpi, making glycerol-phosphate depletion among the earliest known effects of HCMV infection on cellular metabolism. Taken together, these results demonstrate that HCMV infection depletes a subset of precursor metabolites, some very rapidly, most likely utilizing them for its own macromolecular synthesis.

Taurine, an amino acid analog involved in osmoregulation and cell volume control [32], is not an obvious precursor metabolite, but was nevertheless decreased 4-fold by HCMV infection (Figure 6, top left panel). Typically, if a cell is subjected to hypo-osmotic conditions, taurine is rapidly transported out of the cell to compensate for the osmotic imbalance and to prevent cell volume increase [32,33]. The cytomegaloviruses are named for the cytopathic effect they induce, which involves a significant increase in cell volume. It seems likely that taurine is not utilized by the virus, but instead excreted by the host cell in response to the virus-induced increase in cell volume.

HCMV-Induced Metabolite Levels Far Exceed Those Seen in Actively Growing Cells

HCMV activates a number of cyclin-dependent kinases and induces quiescent G0 cells to enter the G1 compartment of the cell cycle and progress to the G1-S border [34,35]. Up to this point, we tested the effects of HCMV infection in confluent, serum-starved G0 cells. Consequently, we were

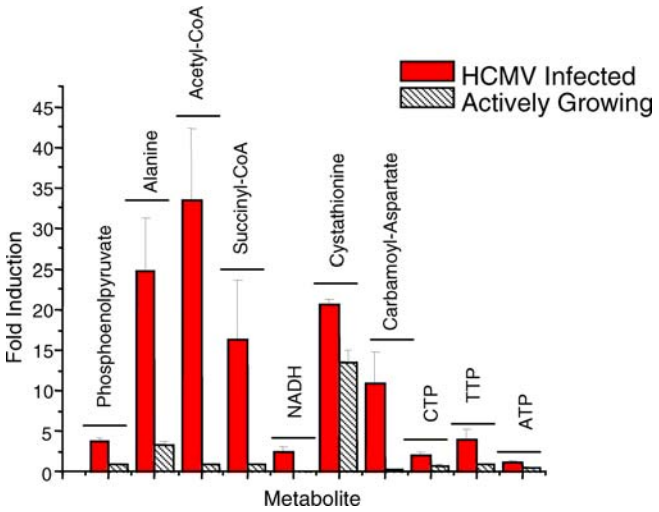

Figure 8. HCMV Infection Disrupts Normal Homeostatic Metabolite Pool Levels

Metabolite levels in HCMV-infected quiescent fibroblasts (72 hpi) and actively growing fibroblasts are reported as fold-induction over quiescent, uninfected cells (mock 4 h). To account for differences in cell count and cell size between conditions, all results are normalized to total protein levels. Bars represent the mean fold-induction from two independent experiments performed in duplicate ($n = 4$), with the error bars showing +1 SE of the mean.

doi:10.1371/journal.ppat.0020132.g008

interested if HCMV-induced metabolic changes mirrored the differences between actively growing and quiescent cells, so we tested how the metabolic changes induced by infection of quiescent G0 cells compared to the differences between quiescent and actively growing cells. Toward this end, we harvested fibroblasts that were actively growing and processed them for LC-MS/MS. Metabolite levels in actively growing fibroblasts were compared to 72-hpi, HCMV-infected fibroblasts. The relative levels of acetyl-CoA, alanine, carbomoyl-aspartate, succinyl-CoA, and to a lesser extent PEP, NADH, CTP, and TTP, were dramatically elevated in HCMV-infected fibroblasts compared to actively growing fibroblasts (Figure 8). Thus, HCMV does not modify the cellular metabolome simply by inducing quiescent cells to enter the G1 phase of the cell cycle. Rather, the virus reprograms the metabolic status of the cell, producing a unique signature of infection.

Conclusions and Future Directions

The network of chemical reactions involving the derivation of energy currency and biosynthetic building blocks from nutrient inputs consists of ~500 different compounds and 700 interconverting reactions [36]. Remarkably, relatively little is known of how intracellular pathogens modulate these metabolites and their interconversions. We utilized a global approach to address this issue. As commonly occurs with such approaches, we generated many specific biochemical hypotheses that necessitate further inquiry. One such hypothesis, that HCMV infection induces phosphofrucktokinase activity, was verified. Many more remain untested.

Beyond specific biochemical hypotheses, we also began the process of tackling larger biological questions regarding the metabolic interplay between pathogens and their hosts. Can pathogens meet their biosynthetic needs simply by activating cellular growth pathways with a coordinate increase in metabolic activity? This does not appear to be the case for HCMV. Our results indicate that the virus institutes its own metabolic program, altering normal metabolic homeostasis maintained in quiescent and growing cells and considerably stimulating aspects of glycolysis, the citric acid cycle, and pyrimidine biosynthetic metabolic pathways. Future experiments are necessary to determine whether the numerous metabolic differences observed during HCMV infection are necessary for efficient viral replication, and, if so, the means by which these metabolic alterations contribute to the virus growth cycle.

Materials and Methods

Biological reagents. Primary human foreskin fibroblasts (passages 6–10) were cultured in Dulbecco's modified Eagle medium (DMEM) containing 7.5% fetal calf serum and 4.5 g/L glucose. All infections were carried out with BAD*wt,* which is derived from a bacterial artificial chromosome (BAC) clone of the AD169 strain of HCMV [37]. The BAC was inserted into the genome of HCMV without deletion of any viral sequence and was excised by a co-transfected CRE recombinase that mediates recombination at the loxP sites, which flank the BAC, leaving just the loxP site in the viral clone. This clone has been tested in a diversity of assays and has always displayed a wild-type AD169 phenotype.

Cell culture. Fibroblasts were grown to confluence in 10-cm dishes and maintained for 3–5 d, at which time serum-containing medium was removed, and cells were washed once with serum-free DMEM. After maintenance in serum-free DMEM for 24 h, cells were mock infected or infected at a multiplicity of 3.0 pfu/ cell, and after a 2-h adsorption period, the inoculum was aspirated and fresh serum-free medium was added. Cells were harvested for metabolic, transcriptional, or total protein analysis at various times after the initiation of infection. Actively growing non-confluent primary fibroblasts were grown in DMEM containing 7.5% dialyzed fetal calf serum and harvested 24 h after splitting. Flow cytometric analysis of cellular DNA content was performed as previously described [38].

Protein analysis. For total protein analysis, cells were washed with PBS, scraped, pelleted by low speed centrifugation, and solubilized in lysis buffer containing 150 mM KCl, 10 mM Hepes, 1% NP40, 0.5% deoxycholate, 0.1% SDS, 10 μg/ml phenylmethylsulphonylfluoride (PMSF), and 1 μg/ml pepstatin. After 10 min on wet ice, lysates were centrifuged at 14,000 × *g* for 10 min. The protein concentration of supernatant fluids was determined by using the Bradford assay (Bio-Rad Laboratories, http://www.bio-rad.com).

Metabolite extraction. The medium was aspirated from plates containing medium only, actively growing fibroblasts, or fibroblasts that were 4, 24, 48, 72, or 96 h post-mock or post-HCMV infection. Methanol:water 80:20 (80% methanol) at −75 °C was immediately added to quench metabolic activity and extract metabolites. After metabolism quenching, cells were scraped from the plastic tissue culture dish with the dish kept on dry ice, and the resulting cell suspension vortexed, centrifuged at 6000 × *g* for 5 min, and re-extracted twice more with 80% methanol at −75 °C. After pooling the three extractions, the samples were completely dried under nitrogen gas, dissolved in 200 μl 50% methanol, and spun at 13,000 × *g* for 5 min to remove debris. Internal standard mix (15 μl) was added to an aliquot of the supernatant (135 μl) and the mixture was analyzed by LC-MS/MS as described below with the virally infected and mock-infected samples alternated (to avoid artifacts in the measurement of unstable compounds due to differential processing times), and all analyses completed within 16 h of sample collection (to further mitigate any potential problems with sample stability). The internal standard mix was comprised of ^{13}C-,^{15}N-labeled compounds (uniformly labeled unless otherwise indicated, from Cambridge Isotope Laboratories, http://www.isotope.com; or Medical Isotopes, http://www.medicalisotopes.com) in 50% methanol with 0.1% formic acid: ATP (2 μg/ml), TTP (2 μg/ml), succinate (1,4-^{13}C, 1 μg/ml), threonine (1 μg/ml), glutamate (1 μg/ml), UMP (1 μg/ml), AMP (1 μg/ml), and deoxyadenosine (0.1 μg/ml).

Phosphofrucktokinase assay. 48 h post-mock or post-HCMV infection, cells were washed once and then scraped into ice- cold PBS. After centrifugation at 1,000 × *g* for 5 min, cell pellets were resuspended in 200 μl 60 mM Hepes (pH 7.4), 1 mM $MgCl_2$, 5 mM DTT, 0.6 mM PMSF, and 40 mM NaF. Cellular suspensions were

freeze-thawed three times and centrifuged at 13,000 × *g* for 10 min to remove insoluble debris. ATP (final concentration 1.8 mM), iodoacetate (final concentration 150 μM), and fructose 6-phosphate (final concentration 1.8 mM) were added immediately, prior to starting the reaction by incubation at 37 °C, with the iodoacetate serving to inhibit the downstream glycolytic enzyme, glyceraldehyde 3-phosphate dehydrogenase. Reactions were stopped at various times by sampling 20 μl and adding 120 μl 80% methanol. Samples were spun at 13,000 × *g* for 5 min to remove debris. Internal standard mix (15 μl) was added to an aliquot of the supernatant (120 μl) and the mixture was analyzed for FBP accumulation by LC-MS/MS as described below. The resulting data were fit to a single-exponential curve describing saturable product formation with pseudo first-order kinetics:

$$S(t) = S_{max}(1 - e^{-kt})$$

(This maximally simple curve fit approximates Michaelis-Menten kinetics for a single substrate with $K_m >$ [substrate].) The data fit the curve very well for both the infected ($R^2 = 0.998$) and uninfected samples ($R^2 = 0.993$), with S_{max} values equal to 2.3×10^4 (infected) and 3.5×10^4 (uninfected) and an ~6-fold difference in k (0.0405 ± 0.002 versus 0.0066 ± 0.001), which translates into a corresponding ~4-fold difference in initial velocity given the proportionality of initial velocity to $k*S_{max}$.

LC-MS/MS instrumentation. LC-MS/MS was performed using an LC-10A HPLC system (Shimadzu, http://www.shimadzu.com) and a Luna aminopropyl column (250 mm × 2 mm with a 5-μm particle size from Phenomenex, http://www.phenomenex.com) coupled to the mass spectrometer. The LC parameters were as follows: autosampler temperature, 4 °C; injection volume, 20 μL; column temperature, 15 °C; and flow rate, 150 μL/min. The LC solvents were Solvent A: 20 mM ammonium acetate + 20 mM ammonium hydroxide in 95:5 water:acetonitrile (pH 9.45); and Solvent B: acetonitrile. The gradients are as follows: positive mode—t = 0, 85% B; t = 15 min, 0% B; t = 28 min, 0% B; t = 30 min, 85% B; t = 40 min, 85% B; and negative mode—t = 0, 85% B; t = 15 min, 0% B; t = 38 min, 0% B; t = 40 min, 85% B; t = 50 min, 85% B.

Mass spectrometric analyses were performed on a Finnigan TSQ Quantum Ultra triple-quadrupole mass spectrometer (Thermo Electron Corporation, http://www.thermo.com), equipped with an electrospray ionization (ESI) source. ESI spray voltage was 3,200 V in positive mode and 3,000 V in negative mode. Nitrogen was used as sheath gas at 30 psi and as the auxiliary gas at 10 psi, and argon as the collision gas at 1.5 mTorr, with the capillary temperature 325 °C. Scan time for each SRM transition was 0.1 s with a scan width of 1 m/z. The LC runs were divided into time segments, with the SRM scans within each time segment limited to those compounds eluting during that time interval. For compounds eluting at the boundaries between time segments, the SRM scan corresponding to the compound is conducted in both time segments. The instrument control, data acquisition, and data analysis were performed by the Xcalibar software (Thermo Electron Corporation, version 1.4 SR1), which also controlled the chromatography system.

Metabolite data analysis. To quantify metabolite levels, peak heights for 167 different metabolite SRMs were determined for each sample. A metabolite was not analyzed further if: (i) its signal for all viral and mock samples was undetectable; (ii) its maximum signal for all viral or mock samples was less than 5-fold that of the maximum signal in the media-alone plates; or (iii) the observed signal likely resulted from a naturally occurring heavy isotope of another metabolite. The last exclusion was implemented, since, if two compounds have similar retention times and fragmentation patterns, the signal for an abundant compound, e.g., AMP, can be potentially mistaken for a less abundant, slightly heavier compound, e.g., IMP, due to naturally occurring ^{13}C, which makes a proportion of AMP heavier and thus potentially contributes to the signal in the IMP SRM. Of the 167 compounds tested, 63 met criteria for further analysis.

Metabolite signal levels represent the average from two different experiments performed in duplicate ($n = 4$). When signals were undetectable or less than 100 for a given sample, they were assigned a signal level of 100, the approximate level of instrument noise. To approximate intracellular concentrations, metabolite signals from each sample were then normalized to 500 μg of total protein (the approximate amount found in the samples) based on the measured total protein level of the corresponding sample (as determined by the Bradford assay). All four measurements (already protein-normalized) taken from the mock-infected cells at 4 h were then averaged to yield a basal signal for each metabolite ($Signal_{basal}$). Fold changes (and their associated SE) relative to this basal signal were then calculated for each sampling time point separately for the viral and mock infection:

$$\text{Fold change} = \frac{\text{Average (Protein-normalized signals for the metabolite}, n = 4)}{\text{Signal}_{basal}}$$

$$\text{SE of fold change} = \frac{\text{SE (Protein-normalized signals for the metabolite}, n = 4)}{\text{Signal}_{basal}}$$

Array analysis. At 4, 24, 48, or 72 h post-mock or post-HCMV infection, medium was aspirated and RNA was prepared using Trizol as recommended by the manufacturer (Invitrogen, http://www.invitrogen.com) and subsequently purified through an RNAeasy column (Quiagen, http://www1.qiagen.com). Fluorescent cRNA (Cy3 and Cy5) was prepared from all samples, as well as a control RNA set (human universal reference total RNA from Clontech, http://www.clontech.com) using the Low RNA Linear Amplification Kit (Agilent, http://www.agilent.com) as per manufacturer's instructions. Independent duplicate samples were dye reversed and sample cRNA was mixed with alternatively labeled (Cy3 versus Cy5) control cRNA and hybridized to Human Whole Genome Oligo Microarray as per the manufacturer's instructions (Agilent). Slides were scanned with an Agilent Scanner (model number G2505B) and data were extracted with Feature Extractor 7.5 software. The resulting data files were imported into Genespring GX 7.3. The recorded fluorescent values were then subjected to the default per-chip and per-gene Lowess normalization with the cross-gene error model active. Only probe sets whose fluorescent signal was flagged as present or unknown were examined. Probe sets were further filtered by control channel expression; all probes with a cRNA control signal of less than 33 fluorescent units were not analyzed further. Analysis of variance (ANOVA) was then performed on the remaining probes using mock versus HCMV infection as the parameter, and grouping the mock 24-, 48-, and 72-h time points together and the HCMV-infected 24-, 48-, and 72-h time points together. The 4-h time points were left out as there was little change between mock- and HCMV-infected metabolic genes at this time point. The Welsh ANOVA analysis was performed using error model variances and Benjamini/Hochberg multiple testing correction with a *p*-value cutoff of 0.05. Probe sets as listed in the text and Figure 7 can be linked with corresponding gene information through: http://www.reactome.org.

Quantitative real-time PCR. RNA used for qRT-PCR was isolated as described above for array analysis. cDNA synthesis was performed utilizing TaqMan Reverse Transcription reagents with random hexamers as per the manufacturer's protocol (Applied Biosystems, http://www.appliedbiosystems.com). qPCR was performed using the Power Sybr Green PCR Master Mix, 7900HT Sequence Detection, and SDS software version 2.1 (Applied Biosystems) following the manufacturer's instructions. Metabolic transcripts were quantified with specific primer pairs as follows: the phosphofructokinase-1 transcript (A__23__P46928) with 5′ AGCTGTATTCAGAAGAGGGCAAAG 3′ and 5′ CCACCCTGCTGCATGTGA3′; the pyruvate dehydrogenase transcript (A__23__P251095) with 5′ GACGAAAAGGAGGTTGT GCTAAAG 3′ and 5′ CCATTGCCCCCGTAGAAGTT 3′; and the pyruvate kinase transcript (A__32__P147241) with 5′ CCGCCTGGA-CATTGATTCAC 3′ and 5′ GGGC CAATGGTACAGATGATG 3′. The GAPDH transcript (A__23__P13899) has been shown to remain constant during HCMV infection [39] and its amplification, with the primers: 5′ ACCCACTCCTCCACCTTTGAC 3′ and 5′-CTGTTGCTGTAGCCAAATTCGT 3′ was used for normalization purposes. Relative quantification with a standard curve for each primer pair was performed as described in the ABI prism 7900HT sequence detection system guide (Applied Biosystems). A dissociation curve was generated for each reaction and demonstrated amplification of a single product. Reactions were performed in duplicate, and non-template controls were included for each primer pair.

Supporting Information

Figure S1. DNA Content of Actively Growing or Quiescent Cells

Found at doi:10.1371/journal.ppat.0020132.sg001 (57 KB PPT).

Figure S2. Isotope-Labeled Internal Standard Controls

Isotope-labeled internal standards were added to mock- (dotted line) and HCMV-infected (red line) samples prior to measurement as described in Materials and Methods. Average SRM peak heights ($n = 4$) and the standard error of their means were plotted relative to the mock 4-hr internal standards on a $\log_2$ axis.

Found at doi:10.1371/journal.ppat.0020132.sg002 (111 KB PPT).

Table S1. Effect of HCMV on Metabolite Levels

Found at doi:10.1371/journal.ppat.0020132.st001 (49 KB XLS).

Table S2. Effect of HCMV on RNA Levels of ATP Syntheses (Mitochondrial Proton Transporting)

Found at doi:10.1371/journal.ppat.0020132.st002 (46 KB PPT).

Acknowledgments

We would like to thank Aster Legesse-Miller and Wenyun Lu for their technical assistance and David Botstein and Manuel Llinas for their helpful comments.

Author contributions. JM, SUB, HAC, TS, and JDR conceived and designed the experiments. JM and SUB performed the experiments. JM and SUB analyzed the data. JDR contributed reagents/materials/analysis tools. JM and JDR wrote the paper.

Funding. This work was supported by a grant from the National Institutes of Health (CA82396 and CA085786) to TS and a NIH Systems Biology Center of Excellence grant (GM71508). JM was supported by a postdoctoral fellowship from the American Cancer Society. JDR was supported by the Beckman Young Investigators program. HAC is grateful for her support from the Rita Allen Foundation as a Milton E. Cassel Scholar.

Competing interests. The authors have declared that no competing interests exist.

References

1. Vancikova Z, Dvorak P (2001) Cytomegalovirus infection in immunocompetent and immunocompromised individuals: A review. Curr Drug Targets Immune Endocr Metabol Disord 1: 179–187.
2. Tanaka S, Furukawa T, Plotkin SA (1975) Human cytomegalovirus stimulates host cell RNA synthesis. J Virol 15: 297–304.
3. Furukawa T, Fioretti A, Plotkin S (1973) Growth characteristics of cytomegalovirus in human fibroblasts with demonstration of protein synthesis early in viral replication. J Virol 11: 991–997.
4. Browne EP, Wing B, Coleman D, Shenk T (2001) Altered cellular mRNA levels in human cytomegalovirus-infected fibroblasts: Viral block to the accumulation of antiviral mRNAs. J Virol 75: 12319–12330.
5. Maharjan RP, Ferenci T (2003) Global metabolite analysis: The influence of extraction methodology on metabolome profiles of *Escherichia coli*. Anal Biochem 313: 145–154.
6. Lu W, Kimball E, Rabinowitz JD (2006) A high-performance liquid chromatography-tandem mass spectrometry method for quantitation of nitrogen-containing intracellular metabolites. J Am Soc Mass Spectrom 17: 37–50.
7. Villas-Boas SG, Hojer-Pedersen J, Akesson M, Smedsgaard J, Nielsen J (2005) Global metabolite analysis of yeast: Evaluation of sample preparation methods. Yeast 22: 1155–1169.
8. Kimball E, Rabinowitz JD (2006) Identifying decomposition products in extracts of cellular metabolites. Anal Biochem 358: 273–280.
9. Bajad SU, Lu W, Kimball EH, Yuan J, Peterson C, et al. (2006) Separation and quantitation of water-soluble cellular metabolites by hydrophilic interaction chromatography-tandem mass spectrometry. J Chromatogr A 1125: 76–88.
10. Kole HK, Resnick RJ, Van Doren M, Racker E (1991) Regulation of 6-phosphofructo-1-kinase activity in ras-transformed rat-1 fibroblasts. Arch Biochem Biophys 286: 586–590.
11. Hue L, Rousseau GG (1993) Fructose 2,6-bisphosphate and the control of glycolysis by growth factors, tumor promoters, and oncogenes. Adv Enzyme Regul 33: 97–110.
12. Hamer MJ, Dickson AJ (1990) Control of glycolysis in cultured chick embryo hepatocytes. Fructose 2,6-bisphosphate content and phosphofructokinase-1 activity are stimulated by insulin and epidermal growth factor. Biochem J 269: 685–690.
13. Landini MP (1984) Early enhanced glucose uptake in human cytomegalovirus-infected cells. J Gen Virol 65: 1229–1232.
14. Hue L, Rider MH (1987) Role of fructose 2,6-bisphosphate in the control of glycolysis in mammalian tissues. Biochem J 245: 313–324.
15. Essen B, Kaijser L (1978) Regulation of glycolysis in intermittent exercise in man. J Physiol 281: 499–511.
16. Newsholme EA, Sugden PH, Williams T (1977) Effect of citrate on the activities of 6-phosphofructokinase from nervous and muscle tissues from different animals and its relationships to the regulation of glycolysis. Biochem J 166: 123–129.
17. Berg JM, Tymoczko JL, Stryer L (2002) Biochemistry. New York: W. H. Freeman. 1,120 p.
18. Mazurek S, Boschek CB, Hugo F, Eigenbrodt E (2005) Pyruvate kinase type M2 and its role in tumor growth and spreading. Semin Cancer Biol 15: 300–308.
19. Chesney J, Mitchell R, Benigni F, Bacher M, Spiegel L, et al. (1999) An inducible gene product for 6-phosphofructo-2-kinase with an AU-rich instability element: Role in tumor cell glycolysis and the Warburg effect. Proc Natl Acad Sci U S A 96: 3047–3052.
20. MacDonald MJ, Al-Masri H, Jumelle-Laclau M, Cruz MO (1997) Oscillations in activities of enzymes in pancreatic islet subcellular fractions induced by physiological concentrations of effectors. Diabetes 46: 1996–2001.
21. Shoaf WT, Jones ME (1973) Uridylic acid synthesis in Ehrlich ascites carcinoma. Properties, subcellular distribution, and nature of enzyme complexes of the six biosynthetic enzymes. Biochemistry 12: 4039–4051.
22. Mori M, Ishida H, Tatibana M (1975) Aggregation states and catalytic properties of the multienzyme complex catalyzing the initial steps of pyrimidine biosynthesis in rat liver. Biochemistry 14: 2622–2630.
23. Coleman PF, Suttle DP, Stark GR (1977) Purification from hamster cells of the multifunctional protein that initiates de novo synthesis of pyrimidine nucleotides. J Biol Chem 252: 6379–6385.
24. Tatibana M, Ito K (1969) Control of pyrimidine biosynthesis in mammalian tissues. I. Partial purification and characterization of glutamine-utilizing carbamyl phosphate synthetase of mouse spleen and its tissue distribution. J Biol Chem 244: 5403–5413.
25. Ito K, Nakanishi S, Terada M, Tatibana M (1970) Control of pyrimidine biosynthesis in mammalian tissues. II. Glutamine-utilizing carbamoyl phosphate synthetase of various experimental tumors: Distribution, purification, and characterization. Biochim Biophys Acta 220: 477–490.
26. Sigoillot FD, Kotsis DH, Serre V, Sigoillot SM, Evans DR, et al. (2005) Nuclear localization and mitogen-activated protein kinase phosphorylation of the multifunctional protein CAD. J Biol Chem 280: 25611–25620.
27. Serre V, Guy H, Liu X, Penverne B, Herve G, et al. (1998) Allosteric regulation and substrate channeling in multifunctional pyrimidine biosynthetic complexes: Analysis of isolated domains and yeast-mammalian chimeric proteins. J Mol Biol 281: 363–377.
28. Scully JL, Evans DR (1991) Comparative modeling of mammalian aspartate transcarbamylase. Proteins 9: 191–206.
29. Penverne B, Belkaid M, Herve G (1994) In situ behavior of the pyrimidine pathway enzymes in *Saccharomyces cerevisiae*. 4. The channeling of carbamylphosphate to aspartate transcarbamylase and its partition in the pyrimidine and arginine pathways. Arch Biochem Biophys 309: 85–93.
30. Vaz FM, Wanders RJ (2002) Carnitine biosynthesis in mammals. Biochem J 361: 417–429.
31. Foster DW (2004) The role of the carnitine system in human metabolism. Ann N Y Acad Sci 1033: 1–16.
32. Lambert IH (2004) Regulation of the cellular content of the organic osmolyte taurine in mammalian cells. Neurochem Res 29: 27–63.
33. Thurston JH, Hauhart RE, Naccarato EF (1981) Taurine: Possible role in osmotic regulation of mammalian heart. Science 214: 1373–1374.
34. Dittmer D, Mocarski ES (1997) Human cytomegalovirus infection inhibits G1/S transition. J Virol 71: 1629–1634.
35. Hayashi ML, Blankenship C, Shenk T (2000) Human cytomegalovirus UL69 protein is required for efficient accumulation of infected cells in the G1 phase of the cell cycle. Proc Natl Acad Sci U S A 97: 2692–2696.
36. Ouzounis CA, Karp PD (2000) Global properties of the metabolic map of *Escherichia coli*. Genome Res 10: 568–576.
37. Yu D, Smith GA, Enquist LW, Shenk T (2002) Construction of a self-excisable bacterial artificial chromosome containing the human cytomegalovirus genome and mutagenesis of the diploid TRL/IRL13 gene. J Virol 76: 2316–2328.
38. Coller HA, Sang L, Roberts JM (2006) A new description of cellular quiescence. PLoS Biol 4: e83. doi:10.1371/journal.pbio.0040083
39. Reinhardt B, Schaarschmidt P, Bossert A, Luske A, Finkenzeller G, et al. (2005) Upregulation of functionally active vascular endothelial growth factor by human cytomegalovirus. J Gen Virol 86: 23–30.